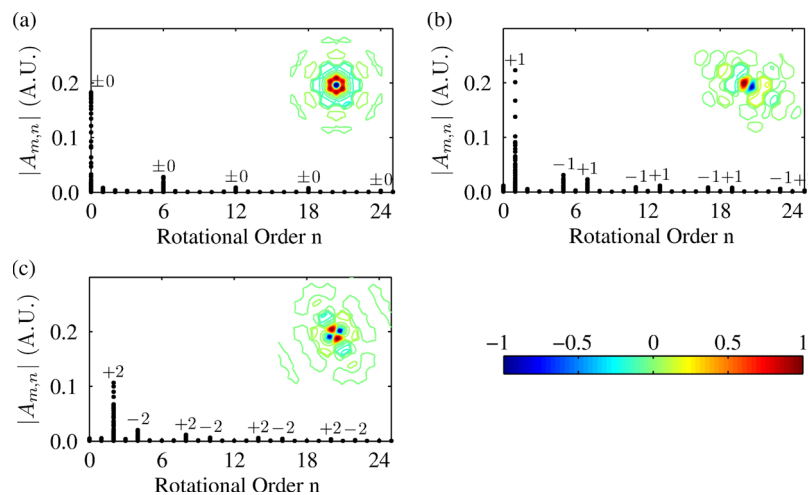# Representation of Photonic Crystals and Their Localized Modes Through the Use of Fourier–Bessel Expansions

Volume 3, Number 6, December 2011

S. R. Newman
G. C. Gauthier

Representation of Photonic Crystals and Their Localized Modes Through the Use of Fourier–Bessel Expansions

S. R. Newman and G. C. Gauthier

Department of Electronics, Carleton University, Ottawa, ON K1S 5B6, Canada

Abstract: Photonic crystal (PhC) geometry is typically characterized by its translational symmetry. However, it can be treated based on the rotationally symmetry through the use of Fourier–Bessel expansions about the center of rotation. Fourier–Bessel expansions of the inverse dielectric of the structures and the transverse electric (TE) localized modes extract the rotational symmetry that is present. The results show that in PhCs and photonic quasi-crystals, the localized H_z field contains only the rotational orders that correspond to the rotational order of the dielectric plus and minus the rotational order of the corresponding perfect state. This relationship indicates the potential for simplification within the master equation in cylindrical coordinates that will require further examination.

Index Terms: Photonic crystals, nanocavities, modeling.

1. Introduction

As photonic crystal (PhC) technology has matured, there have been many models and techniques developed in order to analyze the resulting structures, these include scattering matrix solutions [1], [2], the plane-wave expansion method (PWEM) [3], and the finite difference time domain (FDTD) [4]–[6]. While the FDTD method is capable of handling any dielectric layout, in both 2-D and 3-D, its use generally requires significant computational resources. The more efficient PWEM relies on the existence of a unit cell with a translationally symmetric lattice to calculate the band structure of the PhC. The difficulty arises in the use of PWEM when the PhC in question is disordered or is a photonic quasi-crystal that possesses only rotational symmetry [7]–[9]. Rotational symmetry is not unique to photonic quasi-crystals; within translationally symmetric structures, there are centers of rotation, about which a number of repetitions or folds occur within 2π. By this definition of rotational symmetry, the square and triangular lattices can be expressed as four- and six-fold rotational structures, respectively. The shape of the localized modes within the PhCs will be dependent on the rotational symmetry of the structure, as required by the wave equation.

Within the 2-D plane (r, θ) of the cylindrical coordinate system, the Fourier–Bessel expansion is used in the same manner as the Fourier expansion in Cartesian coordinates. Fourier–Bessel expansions have found use in the scattering matrix models of PhCs in the expansion and characterization of the scattered fields from cylindrical scatterers [1]. Fourier–Bessel analysis has also been used in the study of patterns in a circular domain [10]. In this paper, the Fourier–Bessel expansion will be used to examine the relationship between the rotational order of the dielectric
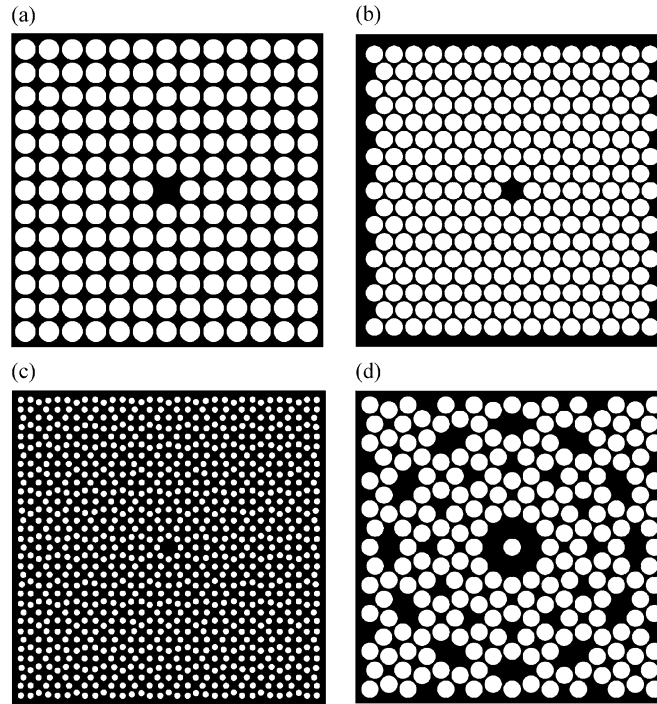
Fig. 1. Structures under investigation (a) Square lattice (with a missing hole as the central lattice defect), (b) triangular lattice (with central lattice defect), (c) eight-fold quasi-crystal (with central defect), and (d) 12-fold quasi-crystal. All four structures are air holes (white, $\epsilon_r = 1.00$) in a silicon (black, $\epsilon_r = 12.1104$) background.

layout of PhCs and the H_z component of the TE states present. The nature of the rotational symmetry will be explored within the traditional four-fold (square) and six-fold (triangular) followed by the eight-fold and 12-fold quasi-crystal structures (see Fig. 1). All four structures are 2-D, r, and θ and are considered invariant along the z axis. The first three structures contain centered defects in the form of missing holes in order to introduced localized states. The 12-fold photonic quasi-crystal contains localized modes without requiring defects [9]. The paper will be structured in the following manner such that Section 2 will introduce the F–B expansion and its use in the decomposition of the inverse dielectric of the structures under examination. Section 3 will examine the decomposition of the localized states present within the photonic crystal and quasi-crystal structures. Section 4 will explore the significance of the rotational order in the states in the context of the wave equation and its potential simplification.

2. Fourier–Bessel Expansion and Rotational Symmetry

In the translationally symmetric PhCs, the dielectric, and field within the wave equation [11], (1), shown below, can be expanded using Fourier analysis, which is the PWEM for PhCs

$$\nabla \times \left(\frac{1}{\epsilon(\mathbf{r})} \nabla \times \mathbf{H}(\mathbf{r}) \right) = \left(\frac{\omega}{c} \right)^2 \mathbf{H}(\mathbf{r}). \tag{1}$$

For 2-D rotationally symmetric structures, it is reasonable to expand the curl in (1) in the cylindrical coordinate system. The H_z field expansion for the TE polarized modes is

$$\frac{1}{r} \left(\frac{\delta}{\delta r} \left[r\Omega \left(-\frac{\delta H_z}{\delta r} \right) \right] - \frac{d\delta}{\delta \theta} \left[\frac{\Omega}{r} \frac{\delta H_z}{\delta \theta} \right] \right) = \left(\frac{\omega}{c} \right)^2 H_z \tag{2}$$

where $\Omega = 1/\epsilon$ is used to simplify the equation. While inverting the dielectric will affect the values obtained for expansion coefficients, it will not change the symmetry as the location of features, i.e.,

the holes, have not changed relative to the background. Following the example of Fourier analysis in the PWEM, the field and inverse dielectric can be expressed in terms of Fourier–Bessel expansions. The Fourier–Bessel expansion is an expression of a given function in both radial, Bessel and angular, exponential components using

$$f(r, \theta) = \sum_{m=0}^{\infty} \sum_{n=-\infty}^{\infty} c_{m,n} J_\alpha\left(\frac{z_m r}{b}\right) e^{jn\theta} \tag{3}$$

where $c_{m,n}$ are the expansion coefficients, α is the order of the Bessel function, and z_m is the mth zero of J_α. The orthonormality and completeness of the Fourier–Bessel expansions allow for the expression for the expansion coefficients to be given as [10]

$$c_{m,n} = \frac{\int_0^{2\pi} \int_0^b rf(r, \theta) J_\alpha\left(\frac{z_m r}{b}\right) e^{-jn\theta} \, dr \, d\theta}{\pi b^2 (J_{\alpha+1}(z_m))} . \tag{4}$$

Using (4), the expansion for H_z and Ω can be expressed as

$$H_z = \sum_{m=0}^{M} \sum_{n=-N}^{N} A_{m,n} J_\alpha\left(\frac{z_m r}{b}\right) e^{jn\theta} \tag{5}$$

$$\Omega = \sum_{p=0}^{P} \sum_{q=-Q}^{Q} B_{p,q} J_\alpha\left(\frac{z_p r}{b}\right) e^{jq\theta} \tag{6}$$

where the complete series requires that $M, N, P,$ and Q be ∞. In this fashion, the rotational order of both H_z and Ω can be extracted through the indices of n and q, respectively. The structures under examination (see Fig. 1) are 10 μm $\times$ 10 μm arrays of air holes $\epsilon_r = 1.00$ in a silicon background $\epsilon_r = 12.1104$. The structures were discretized at 120 pts/μm in Cartesian coordinates. The square and triangular lattices were chosen to have lattice constants a of 630 nm and an $r/a = 0.43$. These lattice parameters provide bandgaps and localized modes approximately centered around the 1.55-μm range. During FDTD simulations, the structures were excited with a noise source that was sufficiently random to excite the localized states [12]. The two photonic quasi-crystals were generated using an algorithm reproducing the structures obtained through dual beam holographic lithography [8]. The spacing between the planes in each exposure allow control over the scaling of the pattern. The eight-fold photonic quasi-crystal design required a plane spacing of 0.417 μm, while the 12-fold quasi-crystal required a plane spacing of 0.8 μm. The scaling of the quasi-crystals was chosen to ensure that their bandgaps and localized modes, along with the square and triangular lattices, were about the chosen wavelength range. When the inverse dielectric and fields were to be expanded in cylindrical coordinates, they were discretized with 280 pts/μm along r and 720 pts/π along θ. A four-point Taylor series was used to extract values for (r, θ) grid points that did not perfectly align with the (x, y) discretized FDTD grid.

Figs. 2–5 present the angular component of Ω of the expansions of the dielectric structures with the inserts showing the Ω layout. The Fourier–Bessel expansions $P = 100$ and $Q = 100$ were performed over a 9.5-μm diameter circle about the center of rotational symmetry. In order to focus on the angular symmetry, the magnitude of the expansion coefficients are plotted such that all the radial components are overlapped at their rotational order. Each order q has 100 points for the 100 radial components p used in the expansion. While not presented here, the expansion coefficients were used in the Fourier–Bessel expressions to reconstruct the inverse dielectric profile to verify the expansion. Convergence tests determined that a larger number of Fourier–Bessel terms improved reconstruction accuracy but did not introduce terms that contradicted the symmetries established when P and Q were set to 100.

The square lattice PhC is a four-fold structure; it is expected that there should be coefficients at this rotational order $q = 4$ in the expansion; see Fig. 2. While this is the case, there are additional
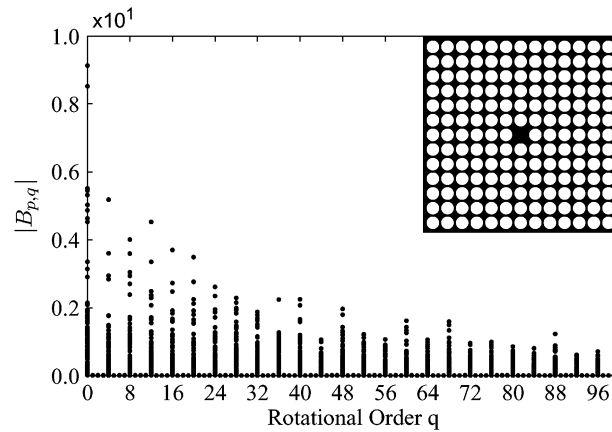
Fig. 2. Fourier–Bessel expansion of 9.5-μm diameter circle of the dielectric layout (inset) of the square lattice showing the rotational symmetry in multiples of 6 present within the structure.
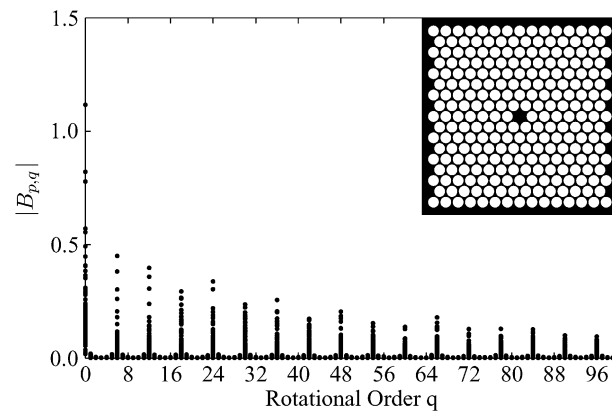

Fig. 3. Fourier–Bessel expansion of 9.5-μm diameter circle of the dielectric layout (inset) of the triangular lattice showing the rotational symmetry in multiples of 6 present within the structure.
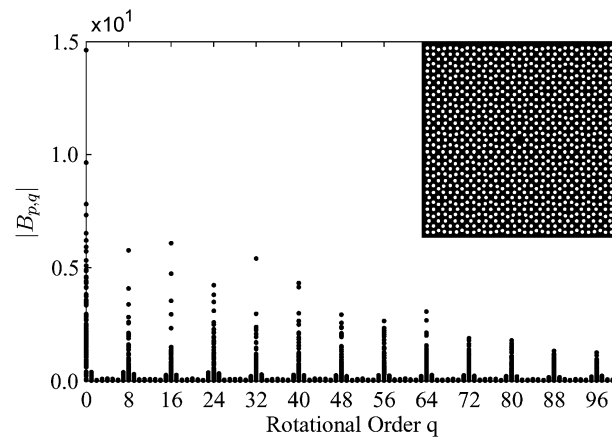

Fig. 4. Fourier–Bessel expansion of 9.5-μm diameter circle of the dielectric layout (inset) of the eight-fold photonic quasi-crystal lattice showing the rotational symmetry in multiples of 8 present within the structure.
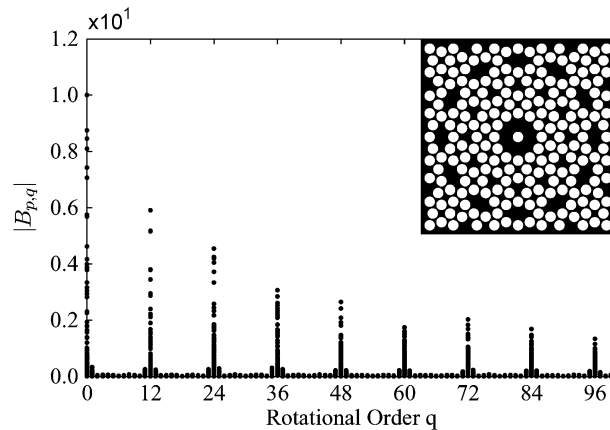
Fig. 5. Fourier–Bessel expansion of 9.5-μm diameter circle of the dielectric layout (inset) of the 12-fold photonic quasi-crystal lattice showing the rotational symmetry in multiples of 12 present within the structure.

nonzero coefficients. This lattice is not a pure four-fold structure; moving radially out, there are regions containing rotational orders that are multiples of the fundamental four-fold symmetry (8, 12, 16, . . .). The Fourier–Bessel analysis introduces additional features into the expansion. As with standard Fourier analysis, the coefficients for terms where the expansion is 1, e^0 are used to establish a background that is then modified by subsequent terms. This can be seen in Fig. 2 with the presence of the $B_{p,0}$ coefficients. Another feature introduced through the Fourier analysis is the presence of harmonics of the fundamental rotational order. As the structure to be expanded, in this case a step function, deviates from a sinusoidal, harmonics are introduced, contributing to the presence of coefficients at multiples of the fundamental rotational order. The final feature in the expansion is the lack of one- or two-fold symmetry. These orders are suppressed due to their destructive interaction with the sinusoidal component of the Fourier–Bessel expansion. It should also be noted that the $B_{p,0}$ coefficients are the only ones affected by the absence of the central air hole as this defect has no angular dependence. The six-fold triangular lattice (see Fig. 3) only has nonzero coefficients at multiples of the six-fold rotational symmetry, matching the results shown with the square lattice. Unlike the square lattice, the expansion of the triangular lattice contains sidelobes to the principal orders of expansion. When the Taylor series is used to map the Cartesian grid to cylindrical coordinates, it results in grid points having values of $\epsilon_o \epsilon_r$ where the relative dielectric constant ϵ_r is not $\epsilon_r = 1$ or 12.1104, grading the edges of the features. This rounding of the step function that previously described the dielectric results in the sidelobes within the Fourier–Bessel expansions. While both the square and triangular lattices have the same r/a, the triangular lattice has a higher filling ratio [see Fig. 1(a) and (b)], resulting in smaller dielectric veins between the holes. The smaller dielectric features enhance the effects of the grading resulting in larger sidelobes. The resolutions used in this study are sufficient to correctly model the dielectric lattices as the FDTD results were verified through convergence tests. While discretization of the dielectric grid in cylindrical (r, θ) coordinates removed the presence of sidelobes, the FDTD simulations, which are results for localized modes, were in Cartesian coordinates. The dielectric was initially discretized in Cartesian coordinates and then converted to cylindrical to remain consistent with the procedure required for the expansions of the localized modes. A further extension of the use of the Fourier–Bessel expansion is its application to the eight- and 12-fold photonic quasi-crystals, which only possess rotational symmetry; see Figs. 4 and 5. Both of the quasi-crystal structures demonstrate that the nonzero expansion coefficients occur when the rotational order q is a multiple order of the fundamental symmetry. Both structures also show evidence of the average background inverse dielectric expansions at $B_{p,0}$. The structures in this study show that if a given inverse dielectric is expanded about its center of rotation with Fourier–Bessel expansions, then the
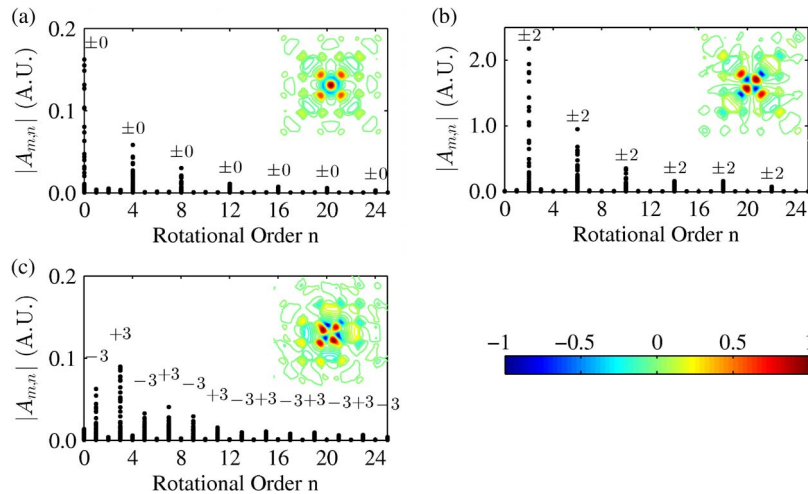
Fig. 6. Fourier–Bessel expansion of the three localized state in the square lattice. The states present are the (a) monopole, (b) quadrupole, and (c) skewed hexapole. Field profiles are shown in contour plots in insets. Decomposition is on a circle with a diameter of 9.5 μm about the center of the lattice.

rotational orders present can be extracted. In this context, it is the rotational symmetry that is common to both the traditional PhCs and the quasi-crystals examined here.

3. Rotational Symmetry Within Localized States

To proceed with the expansions of the localized states and their comparison with the inverse dielectric results, it is necessary to ensure that the four structures have localized modes. The two translational structures, as well as the eight-fold quasi-crystal, required defects in the form of the center air hole missing; see Fig. 1. A lattice defect was not necessary with the 12-fold quasi-crystal as the central localized modes are naturally present within this structure [9]. The field amplitudes calculated through FDTD simulations were scaled to range from -1 to 1 prior to the Fourier–Bessel expansion. The scaling was necessary to place the fields on relative scales as they are not equally excited by the FDTD noise source.

The examination of the rotational order present within available localized states begins with the square lattice. The lowest rotational order states, obtained through FDTD simulations, present in this structure are the monopole, quadrupole, and a skewed hexapole; see the insets of Fig. 6(a)–(c), respectively. The inserts are focused on the center 4.7 μm $\times$ 4.7 μm region of the fields. By its very nature, the perfect monopole does not have an angular dependence. When expanded using Fourier–Bessel, the coefficients would have angular orders $n_{\text{perfect}} = 0$ causing the exponential terms in the expansion to equal 1. The expansion of the localized monopole-like state obtained with the square lattice [see Fig. 6(a)] shows nonzero peaks at multiples of the fundamental order of the dielectric. The rotational order of the monopole-like localized state takes on the rotational order characteristic of the rotational order of the inverse dielectric.

When a perfect quadrupole is examined, the exponential terms would contain $n_{\text{perfect}} = \pm2$. The expansion of the quadrupole-like state obtained with the square lattice shows nonzero coefficients for rotational orders at $n = \{2, 6, 10, 14, \ldots\}$ These particular $A_{m,n}$ coefficients are the multiples of the fundamental rotational order of the inverse dielectric, i.e., $q = \{4, 8, 12, \ldots\}$, each offset by $n_{\text{perfect}} = \pm2$, $n = \{0 \pm 2, 4 \pm 2, 8 \pm 2, \ldots\}$, as indicated in the figure. The third state is a skewed hexapole-like state $n_{\text{perfect}} = \pm3$ with a slight dipole bias $n_{\text{perfect}} = \pm1$. Geometrically, a hexagonal state should have its features distributed about a circle relative to the defect. Examination of the state [see the insert in Fig. 6(c)] shows that while it does have the $n_{\text{perfect}} = \pm3$ order of a hexapole, it is distributed about an oval. Based on the oval nature of the state and the expansion, the rotational order of the mode could be described as either $n_{\text{perfect}} = \pm3$ or ± 1, i.e., $4 - 1 = 0 + 3$. The dominant contribution to the expansion coefficients must come from the rotational orders corresponding
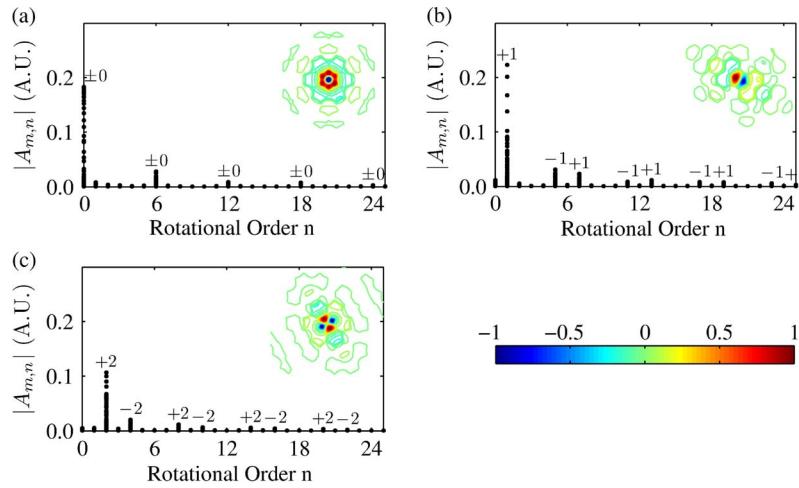
Fig. 7. Fourier–Bessel expansion of the three localized state in the triangular lattice. The states present are the (a) monopole, (b) dipole, and (c) quadrupole. Field profiles are shown in contour plots in insets. Decomposition is on a circle with a diameter of 9.5 μm about the center of the lattice.
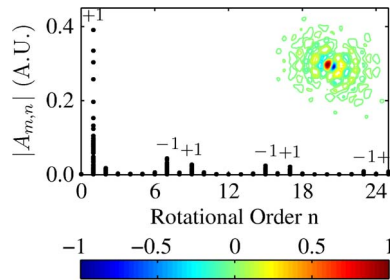

Fig. 8. Fourier–Bessel expansion of the dipole localized state in the eight-fold photonic quasi-crystal lattice. Field profiles are shown in contour plots in insets. Decomposition is on a circle with a diameter of 9.5 μm about the center of the lattice.

to ± 3 as the state profile is predominantly a hexagonal state. Based on the observation that the dominant rotational orders are from the $n_{\text{perfect}} = \pm 3$ coefficients, it should be noted that the $n = +3$ orders reach a higher maximum amplitude than the $n = -3$ within a single rotational order of the inverse dielectric, in this case 4. For example, the $A_{m,3}$ coefficients have a higher maximum amplitude than the $A_{m,1}$ coefficients. The lowest rotational modes present within the triangular lattice are the monopole ($n_{\text{perfect}} = \pm 0$), dipole ($n_{\text{perfect}} = \pm 1$), and the quadrupole ($n_{\text{perfect}} = \pm 2$). The expansions [see Fig. 7(a)–(c)] of the modes show the same behavior that was observed within the square lattice. The rotational orders present within the localized states are the orders of the inverse dielectric layout offset by the symmetry of the perfect state that corresponds to the given localized state. The dipole [see Fig. 7(b)] and the quadrupole [see Fig. 7(c)] also demonstrate that the $A_{m,n}$ components whose radial orders match the positive offset, i.e., $A_{m,1}$ in the dipole, have a higher maximum amplitude than the negative offsets $A_{m,5}$ within a single rotational order of the dielectric. With both the translationally symmetric crystals exhibiting the same trends within their localized states, when expanded about their rotational centers, it would indicate that this behavior is potentially based on the rotational symmetry within these structures and not the translational symmetry. FDTD simulations show that there is a dipole ($n_{\text{perfect}} = \pm 1$) state localized within the eight-fold structure. The Fourier–Bessel expansion of the dipole-like state contains nonzero coefficients at $\{n = 0 \pm 1, 8 \pm 1, \ldots\}$ (see Fig. 8) following the pattern established by the translationally symmetric PhCs. The monopole [see Fig. 9(a)] and hexapole [see Fig. 9(b)] of the 12-fold quasi-crystal follow the results of the other primary states in the other structures, with the hexapole
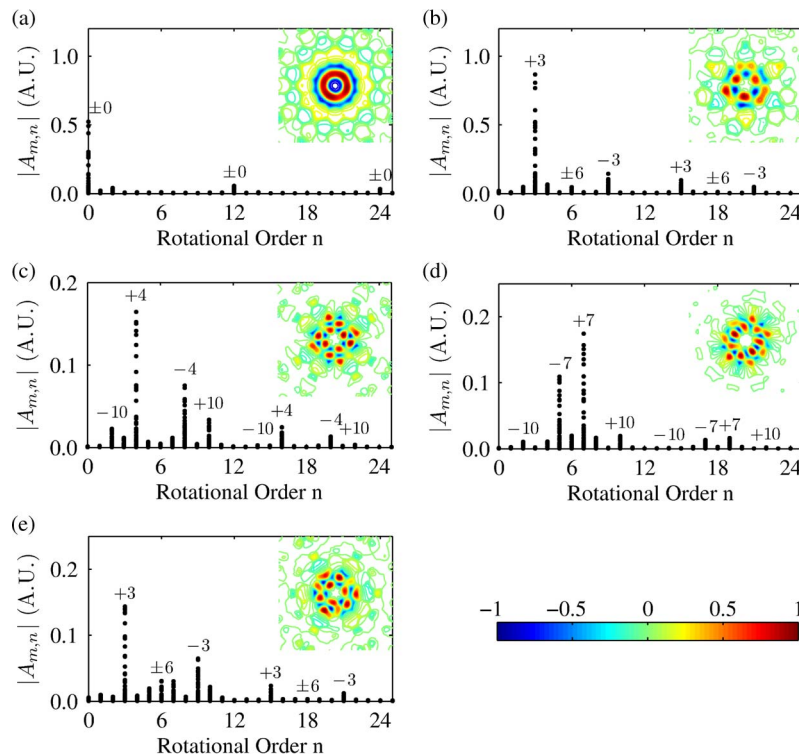
Fig. 9. Fourier–Bessel expansion of the five localized states in the 12-fold photonic quasi-crystal lattice. The states present are the (a) monopole, (b) hexapole and the three states with compound rotational symmetries (c)–(e). Field profiles are shown in contour plots in insets. Decomposition is on a circle with a diameter of 9.5 μm about the center of the lattice.

showing minor contributions from a 12-fold ($n_{\mathrm{perfect}} = \pm6$) state. The more complex modes of the 12-fold structure [see Fig. 9(c) and (d)] are of the same nature as the hexapole-like mode within the square lattice. The difference with these states is that they possess multiple rotational orders such as the $n_{\mathrm{perfect}} = \pm4$ and $n_{\mathrm{perfect}} = \pm10$; see Fig. 9(c). These states also exhibit the behavior related to the maximum amplitudes of the expansion coefficients seen in the localized states within the translationally symmetric structures.

4. Discussion

The Fourier–Bessel expansions show that the rotational order of the H_z field of a localized state possesses a mixing of the rotational symmetry of the inverse dielectric and the corresponding perfect state. As an example, the field of the quadrupole-like state ($n_{\mathrm{perfect}} = \pm2$) in the triangular lattice ($q = 0, \pm6, \ldots$) contains rotational orders of $n = \{\pm1, \pm4, \pm8, \pm10, \pm14, \ldots\}$ or $n = q \pm n_{\mathrm{perfect}}$. All other rotational orders have expansion coefficients of 0.

This knowledge can potentially be used to simplify the process of solving the master equation for the field of a localized state, i.e., H_z in a cylindrical coordinate system. A Fourier–Bessel based solution of the master equation would involve a matrix expression containing the Fourier–Bessel expansions of the inverse dielectric and the field. In the solution for the field of a localized state with a specific profile within a given dielectric layout, the rotational orders that are present for the inverse dielectric q and the field n would be known. The expansion coefficient $A_{m,n}$ is only nonzero when n is a multiple of the fundamental symmetry of the structure, and the expansion coefficient $B_{p,q}$ is only nonzero when $n = q \pm n_{\mathrm{perfect}}$, where n_{perfect} is the rotational order of the perfect state corresponding to the state of interest. Terms with expansion coefficients equal to zero can be left out of the expansions, which will cause matrix elements to be simplified and the order of the matrices to be reduced. These simplifications to the matrix expressions will minimize the number of computations

required to obtain the solution, resulting in lower computation requirements. With reduced computational resources, results could be obtained for a higher resolution or for a larger domain.

5. Conclusion

Through the use of Fourier–Bessel expansions, this paper has shown that the rotational order within the H_z field of the localized modes is the result of a mix between that of the rotational orders of the corresponding perfect state and the dielectric. This interaction has been verified in translationally symmetric structures, square and triangular lattice PhCs, structures lacking translational symmetry, and eight- and 12-fold photonic quasi-crystal. Through these results, it has been shown that in cylindrical coordinates, PhCs with rotational symmetry should be treated the same as rotationally symmetric photonic quasi-crystals. A method of analysis based on the rotational symmetry should prove to be valid for a larger range of crystal structures.

The master equation has also been expressed in cylindrical coordinate to illustrate how it may be simplified through the use of rotational order within the localized modes studied. As these modes have known nonzero expansion coefficients, there is the potential to reduce the number of terms that will need to be evaluated within any potential matrix solution.

Two aspects of this work will require further research and examination. The first is to explore the nature of the role of the rotational order of the dielectric on that of the localized states. The second is the computational solution of the master equation within the cylindrical coordinates in terms of the Fourier–Bessel expansions. This computational technique, when complete, should result in a method that can be used to determine the presence of localized modes in rotationally symmetric photonic lattices, regardless of their translational symmetry.

Acknowledgment

References

[1] G. Tayeb and D. Maystre, Rigorous theoretical study of finite-size two-dimensional photonic crystals doped by microcavities. *J. Opt. Soc. Amer. A, Opt. Image Sci.*, vol. 14, no. 12, pp. 3323–3332, Dec. 1997. [Online]. Available: http://www.opticsinfobase.org/abstract.cfm?URI=josaa-14-12-3323

[2] P. Sabouroux, Experimental and theoretical study of resonant microcavities in two-dimensional photonic crystals. *Opt. Commun.*, vol. 160, no. 1-3, pp. 33–36, Feb. 1999. [Online]. Available: http://linkinghub.elsevier.com/retrieve/pii/S0030401898006427

[3] K. Ho, C. Chan, and C. Soukoulis, Existence of a photonic gap in periodic dielectric structures. *Phys. Rev. Lett.*, vol. 65, no. 25, pp. 3152–3155, Dec. 1990. [Online]. Available: http://link.aps.org/doi/10.1103/PhysRevLett.65.3152

[4] D. M. Sullivan, *Electromagnetic Simulation Using the FDTD Method.* New York: Wiley-IEEE Press, 2000, p. 165. [Online]. Available: http://ieeexplore.ieee.org/xpl/bkabstractplus.jsp?bkn=5263542

[5] A. Taflove and S. C. Hagness, *Computational Electrodynamics: The Finite-Difference Time-Domain Method.* Norwood, MA: Artech House, 2000.

[6] K. Yee, Numerical solution of initial boundary value problems involving Maxwell's equations in isotropic media. *IEEE Trans. Antennas Propag.*, vol. AP-14, no. 3, pp. 302–307, May 1966. [Online]. Available: http://ieeexplore.ieee.org/lpdocs/epic03/wrapper.htm?arnumber=1138693

[7] Y. Chan, C. Chan, and Z. Liu, Photonic band gaps in two dimensional photonic quasicrystals. *Phys. Rev. Lett.*, vol. 80, no. 5, pp. 956–959, Feb. 1998. [Online]. Available: http://link.aps.org/doi/10.1103/PhysRevLett.80.956

[8] R. Gauthier and A. Ivanov, Production of quasi-crystal template patterns using a dual beam multiple exposure technique. *Opt. Express*, vol. 12, no. 6, pp. 990–1003, Mar. 2004. [Online]. Available: http://www.ncbi.nlm.nih.gov/pubmed/19474914

[9] K. Mnaymneh and R. C. Gauthier, Mode localization and band-gap formation in defect-free photonic quasicrystals. *Opt. Express*, vol. 15, no. 8, pp. 5089–5099, Apr. 2007. [Online]. Available: http://www.ncbi.nlm.nih.gov/pubmed/19532759

[10] S. Guan, Fourier–Bessel analysis of patterns in a circular domain. *Phys. D: Nonlinear Phenom.*, vol. 151, no. 2–4, pp. 83–98, May 2011. [Online]. Available: http://linkinghub.elsevier.com/retrieve/pii/S0167278901002238

[11] S. G. Johnson, A. Mekis, S. Fan, and J. D. Joannopoulos, Molding the flow of light. *Comput. Sci. Eng.*, vol. 3, no. 6, pp. 38–47, Nov./Dec. 2001. [Online]. Available: http://ieeexplore.ieee.org/lpdocs/epic03/wrapper.htm?arnumber=963426

[12] S. R. Newman and R. C. Gauthier, FDTD sources for localized state excitation in photonic crystals and photonic quasi-crystals. *Proc. SPIE*, vol. 7223, pp. 72230R–72230R-10, 2009. [Online]. Available: http://link.aip.org/link/PSISDG/v7223/i1/p72230R/s1&Agg=doi